



Validation of Computational Studies for Electrical Brain Stimulation With Phantom Head Experiments



Donghyeon Kim ^a, Jinmo Jeong ^c, Sangdo Jeong ^b, Sohee Kim ^{b,c}, Sung Chan Jun ^{a,*}, Euiheon Chung ^{b,c,**}

^a School of Information and Communications, Gwangju Institute of Science and Technology, 123 Cheomdangwagi-ro, Buk-gu, Gwangju 500-712, South Korea

^b Department of Medical System Engineering, Gwangju Institute of Science and Technology, Gwangju, South Korea

^c School of Mechatronics, Gwangju Institute of Science and Technology, Gwangju, South Korea

ARTICLE INFO

Article history:

Received 14 February 2015

Received in revised form

14 June 2015

Accepted 16 June 2015

Available online 21 July 2015

Keywords:

Electrical brain stimulation

Cortical stimulation

MRI-based phantom head

Computational studies

Validation studies

ABSTRACT

Background: Although computational studies of electrical brain stimulation (EBS) have received attention as a cost-effective tool, few studies have validated the technique, particularly in invasive cortical stimulation.

Objective: In order to validate such studies, we used EBS to compare electric potential distributions generated by both numerical simulations and empirical measurements in three phantom head models (one-/three-layered spherical heads and MRI-based head).

Methods: We constructed spherical phantom heads that consisted of one or three layers, and an anatomical, MRI-based phantom that consisted of three layers and represented the brain or brain/skull/scalp in order to perform both numerical simulations using the finite element method (FEM) and experimental measurements. Two stimulation electrodes (cathode and anode) were implanted in the phantoms to inject regulated input voltage, and the electric potential distributions induced were measured at various points located either on the surface or deep within the phantoms.

Results: We observed that both the electric potential distributions from the numerical simulations and experiments behaved similarly and resulted in average relative differences of 5.4% (spherical phantom) and 10.3% (MRI-based phantom).

Conclusions: This study demonstrated that numerical simulation is reasonably consistent with actual experimental measurements; thus, because of its cost-effectiveness, EBS computational studies may be an attractive approach for necessary intensive/extensive studies.

© 2015 Elsevier Inc. All rights reserved.

Introduction

Electrical brain stimulation (EBS) is a therapy used to modulate or stimulate neural circuits by injecting regulated electrical current/potential into the brain. EBS has long been used to relieve neurological disorders, including essential tremor [1], chronic stroke [2], chronic pain [3], Parkinson's disease [4,5], movement disorders [6], refractory epilepsy [7], depression [8], aphasia [9], and dystonia

This work was supported by the Institute of Medical System Engineering (iMSE) in the GIST, GIST-Caltech Research Collaboration Project through a grant provided by GIST in 2015, a grant from the Integrative Aging Research Center of GIST, and the National Research Foundation (NRF) funded by the Ministry of Education, Science and Technology (2012R1A1A1012853, NRF-2010-0026438).

* Corresponding author. Cheomdangwagi-ro 123, Buk-gu, Gwangju, 500-712, South Korea. Tel.: +82 62 715 2216.

** Corresponding author.

E-mail addresses: scjun@gist.ac.kr (S.C. Jun), ogong50@gist.ac.kr (E. Chung).

[10], among others. Thus, EBS has gained more attention recently in treating brain disorders and brain diseases, and various preclinical animal and human studies have been conducted.

However, despite these animal [11–13] and human studies [14,15], a thorough understanding of the fundamental mechanisms of EBS is still lacking; thus, the stimulation parameters for the best medical practices (electrode position, amplitude, waveform, and duration) remain unclear. In order to resolve this issue, a computational approach has been introduced in EBS. The goal of most computational EBS studies has been to reveal the spatial distributions of the current density or electric field within the brain that are induced by injection of electric current or potential in order to provide better insights in the determination of stimulation parameters. One of the simplest methods involves multi-layered spherical head models that have been introduced into the computational EBS domain. For example, a five-layered spherical head model was used to investigate the magnitude and focus of the

electric field in electroconvulsive therapy and magnetic seizure therapy [16], and the effect of electrode configuration on transcranial direct current stimulation (tDCS) has been investigated in a four-layered spherical head model [17]. Such spherical models have low computational costs and are easy to implement; thus, they may further our knowledge of the effects of stimulation parameters. However, studies have been limited to investigations of the effect of neuromodulation in specific, complicated brain areas. Restricting study to a specific area of the brain, and considering anatomical shape to some extent, extruded slab models that represent the motor cortex have also been generated to investigate the effects of motor cortex stimulation [18–20]. These modeling studies may elucidate the neuromodulation effects in more focused target areas; however, the prediction of overall current density in the whole brain may be misinterpreted due to non-negligibly significant mismatches between these models.

Recently, some efforts have been made to reduce model mismatches by using human magnetic resonance imaging (MRI) and considering anatomical connectivity by incorporating diffusion tensor imaging (DTI) into computational EBS. The current density distribution of tDCS on the individualized brain model generated by patients' MRI data has been investigated [21], and the effects of MRI-based brain geometry on the electric field induced by TMS also have been reported [22,23]. In addition, in a recent study [24], the subdural cortical stimulation (SuCS) effect was estimated in the MRI-based full head model as the magnitude of current density or electric field, with the implicit assumption that the excitability of neurons is linearly proportional to the magnitude of the current density (or electric field). Such approaches have advantages in visualizing overall current density or electric fields in the whole brain and estimating the individualized effects of stimulation, although at an increased computational cost. From a clinical perspective, TMS stimulation effects on stroke patients have been estimated in advance with computational human models [25]. For EBS investigations at a neural level, the association between the spatial deviations in current density (that is, activating function) and neuronal responses has been investigated in computational studies [26,27]. Further, the extracellular responses of L3 and L5 pyramidal neurons induced by cortical stimulation have been investigated in the combined neural compartmental model and full head model [28].

In general, the computational analysis of EBS is based on such numerical techniques as the finite element method (FEM), the finite difference method (FDM), or the boundary element method (BEM). However, in principle, the computational results may be meaningless without reasonable validation; thus, investigations of whether or not they are consistent with experimental results are required. To the best of our knowledge, there are only a few EBS related studies of validation. A DBS study [29] reported that there was qualitative agreement between phantom experimental and numerical results of electrode impedance. Also, according to a TMS computational study [30], the stimulation effects of the geometrical head model, and the conductivity condition and stimulus position of the electric field were validated with a simplified brain-phantom that described the smooth cortex. Furthermore, experimental validation of computational models has been reported in rats in *in-vivo* trans-spinal DCS studies [31], as well as in tDCS studies of humans [32]. Specifically, the human study attempted a direct comparison of computed and measured scalp potentials (EEG), which showed positive correlations and good agreement.

From the above, one can see that, although it is very important to conduct validation studies of EBS, the subject has been investigated rarely. Particularly, validation studies of such computational cortical stimulation techniques as invasive SuCS or EpCS (epidural cortical stimulation) are lacking. Therefore, for the purposes of

validation, we constructed three phantom heads: one-layered and three-layered spherical phantoms, and a human MRI-based phantom. Then, we generated computational head models based on the geometry and properties of these phantom heads, and examined to what degree computational electric potential distributions at designated points on/inside the head models were consistent with distributions measured empirically when regulated input voltage was injected through electrodes implanted on the brain surface of the phantom heads.

Materials and methods

Phantom design

We constructed three phantom heads—a one-layered spherical phantom (representing the brain only), a three-layered spherical phantom, and a human MRI-based three-layered phantom. These were constructed for invasive cortical stimulation with/without skull and scalp, or with simple head/realistic head geometries. To construct the MRI-based phantom, normal human MRI data were obtained, and segmented by *freesurfer* [33] and *fsl* [34] to distinguish the brain, skull, and scalp layers. With these segmented data, a fine mesh consisting of a number of tetrahedrons was generated for FEM analysis. For construction of the MRI-based phantom, several plastic moulds suitable for assembling multi-layer shell structures were built with a 3D printer (Fig. 1A and B). We then made three kinds of Agar/NaCl mixtures with specified electric

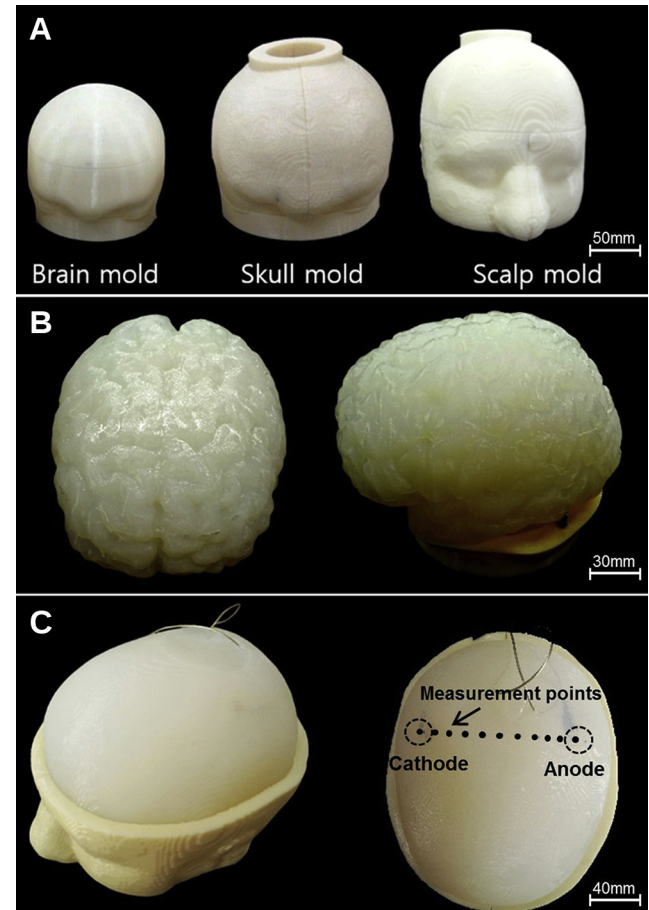


Figure 1. (A) MRI-based phantom head sub-molds representing three layers in the human head. (B) Brain layer generated by brain sub-mold. (C) Assembled phantom with implanted electrodes and measurement (sensing) points.

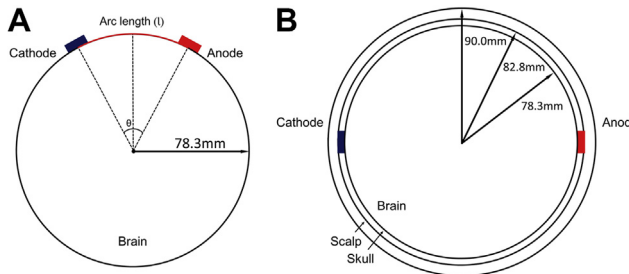


Figure 2. Geometric configuration of the (A) one-layered spherical model and (B) three-layered spherical model.

conductivities [35], which were as close as possible to the isotropic conductivities (scalp, skull, and brain) measured experimentally in humans [36]. In each sub-mould, the corresponding Agar/NaCl mixture was filled and solidified. Two electrodes were placed on the left and right motor cortex areas, and a $1V_{pp}$ (peak-to-peak value of AC voltage with a 1 kHz sine wave changing within 0–1 V) was applied with a function generator (Agilent, E3631A). We note that AC voltage may prevent an oxidation–reduction reaction (redox reaction), which is probably the main cause of changes in electrode impedance during an experiment. After 11 measurement points were obtained between two stimulation electrodes (Fig. 1C), the electric potentials induced by the electrodes were measured with a digital oscilloscope (Agilent, 34410A) from the head surface (a depth of 0 mm) to a depth of 70 mm, in 5 mm increments. To obtain reliable results, we measured each point five times.

The one-/three-layered spherical phantoms were constructed similarly to the three-layered MRI-based phantom. Their geometrical configurations (the radii of spherical shells) are depicted in Fig. 2. The three-layered head model consists of brain, skull, and scalp; the ratio of the spheres' radii was 1:0.92:0.87 (scalp:skull:brain) to mimic the human head [37]. Two ring-type electrodes were attached to opposite sides of the brain surface to mimic invasive cortical stimulation in the spherical head. In this phantom, the measurement procedure was performed in the same manner as in the MRI-based phantom. First, we measured electric potentials at 19 points (0° – 180° , in 10° increments) on the outer sphere representing the scalp. For each point, 11 additional potentials were measured along the line (toward the sphere origin) from the surface (depth of 0 mm) to a depth of 50 mm, in increments of 5 mm. For the one-layered spherical phantom specifically, an angle variation (29.3° , 44.0° , 58.6° , and 180°) between two electrodes was considered; thus, the arc length (l) between two electrodes varied, as illustrated in Fig. 2A. A detailed overall procedure of the phantom head design and comparison strategy is illustrated in Fig. 3.

Computational model

In general, electric neuromodulation involves injecting direct electric current or voltage-induced current into the brain via electrode(s). Maxwell's equation explains such electrical behavior within the brain. The stimulation frequency is relatively low, such that the electromagnetic field induced is quite small. Thus, a quasi-static Maxwell's equation is introduced commonly in computational modeling. Thus, such physical behavior is described as the following Laplacian equation in the model Ω :

$$\nabla \cdot (\sigma \nabla V) = 0 \quad (1)$$

Here, V and σ are an electric potential and an electrical conductivity in Ω , respectively. Assuming that the electric flux from the

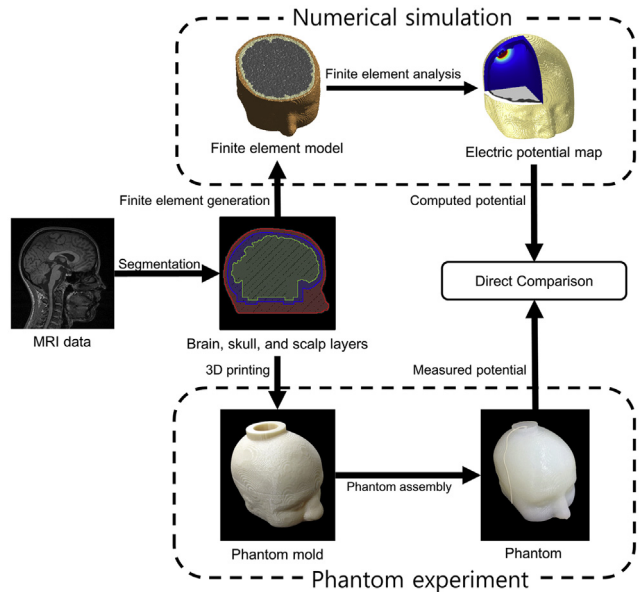


Figure 3. A brief, MRI-based, three-layered phantom head generation and validation procedure.

scalp into the air is negligibly small (that is, insulated), the Neumann boundary condition is applied to the outer boundaries of the scalp, as follows:

$$\mathbf{n} \cdot \mathbf{J} = 0 \quad \text{on } \partial\Omega_{\text{outer}} \quad (2)$$

where \mathbf{n} and \mathbf{J} are normal vectors to the boundary and current density, respectively. Further, Dirichlet boundary conditions are applied at the cathode electrode surface ψ_{cathode} , and the anode electrode surface ψ_{anode} , as follows:

$$V = V_0 \quad \text{on } \partial\psi_{\text{cathode}} \quad (3)$$

$$V = V_1 \quad \text{on } \partial\psi_{\text{anode}} \quad (4)$$

where V_0 and V_1 are input voltages. We note that $V_0 = 0$ V and $V_1 = 1$ V were injected in this present work. We employed the finite element method (FEM) with adaptive tetrahedral volume mesh generation as a computational strategy to solve Equations (1–4) and the boundary value problem. The element volume constraint factor was applied to each model component, so that the mesh was coarse around simple structures, while a finer mesh was used around complex structures. The number of tetrahedral elements was approximately 1.1 million and 1.2 million, respectively, for the one-layered and three-layered spherical head models, and was approximately 3 million for the three-layered MRI based head model (Fig. 4). A bi-conjugate gradient solver with incomplete LU preconditioner was applied as the solver. All simulations were performed using COMSOL Multiphysics 4.3b (COMSOL Inc., Burlington, MA, USA).

Assignment of conductivities

To assign the conductivities of the phantom head to approximate those of an actual human head, we used Agar/NaCl mixtures. The NaCl concentration was varied to adjust the conductivity values specified [35], and three kinds of Agar/NaCl mixtures were generated in this manner. According to the literature, the simple relationship between the electrical conductivity of the Agar/NaCl

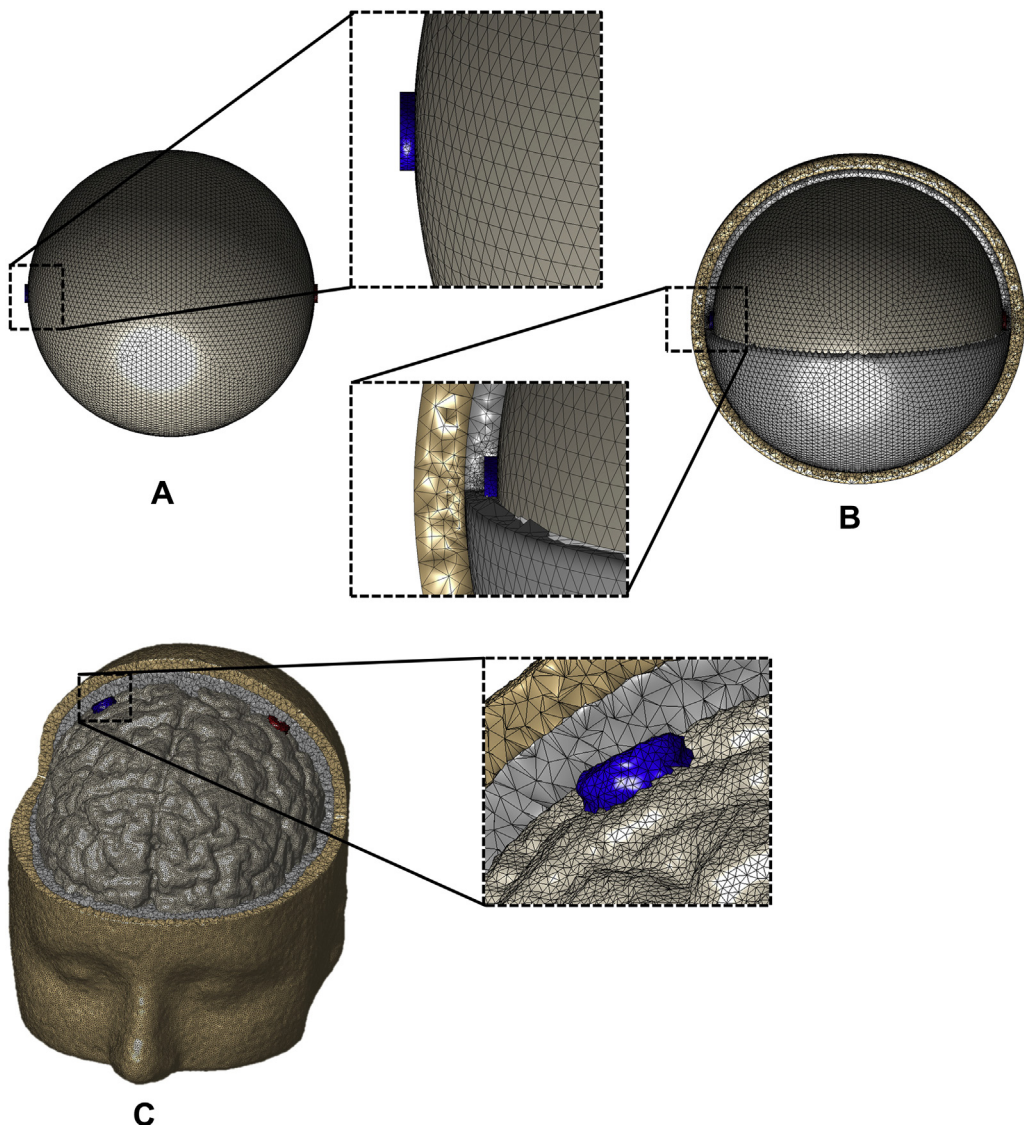


Figure 4. Computational models for (A) one-layered spherical, (B) three-layered spherical, and (C) three-layered MRI-based head models. The spherical models have two electrodes (located the farthest apart) on the outer surface, and the MRI-based model has two electrodes, each located hemispherically on the brain cortex.

mixture and the NaCl concentration may be determined empirically, as follows:

$$\sigma = 215 \times c + 0.0529 \quad (5)$$

Here, σ and c are conductivity (unit: S/m) and NaCl concentration (unit: g/ml), respectively. However, we observed that Equation (5) yielded significantly different conductivity values from the data we measured; this may be due to differences between our Agar powder and its proportion (CAS# 9012-36-6, Affymetrix, 2.6% by weight) and those of Sigma-Aldrich, 0.9% by weight, as used in [35]. As a result, we re-measured electrical conductivity values over various NaCl concentrations (Fig. S1), and generated our modified linear regression model, as follows:

$$\sigma = 179 \times c + 0.032 \quad (6)$$

Note that we used NaCl (Sodium Chloride, CAS# 7647-14-5, DUKSAN, South Korea) and deionized (DI) water to make the NaCl solution. The Agar/NaCl mixtures were manufactured as follows:

first, the NaCl solution was stirred at 40° for 2 h, and then Agar powder was added and stirred with a magnetic stir bar. Finally, the solution was poured into a rectangular-shaped mold, the dimensions of which were 74 mm × 25 mm × 24 mm. The empirical conductivity of the Agar/NaCl mixture was estimated with the following equation:

$$\sigma = I/(A \cdot \Omega) \quad (7)$$

Here, σ , I , and A are conductivity (unit: S/m), length (unit: m), and cross-sectional area (unit: m²), respectively. Ω is the resistance of the Agar/NaCl mixture measured at room temperature with an impedance measurement system (Reference 600, Gamry). Ultimately, we made three kinds of Agar/NaCl mixtures, whose conductivity values were 0.214 (brain layer), 0.012 (skull layer), and 0.470 (scalp layer; S/m). These conductivity values are approximately equal to those of the human head found in the literature [36] (brain: 0.2, skull: 0.01, scalp: 0.465).

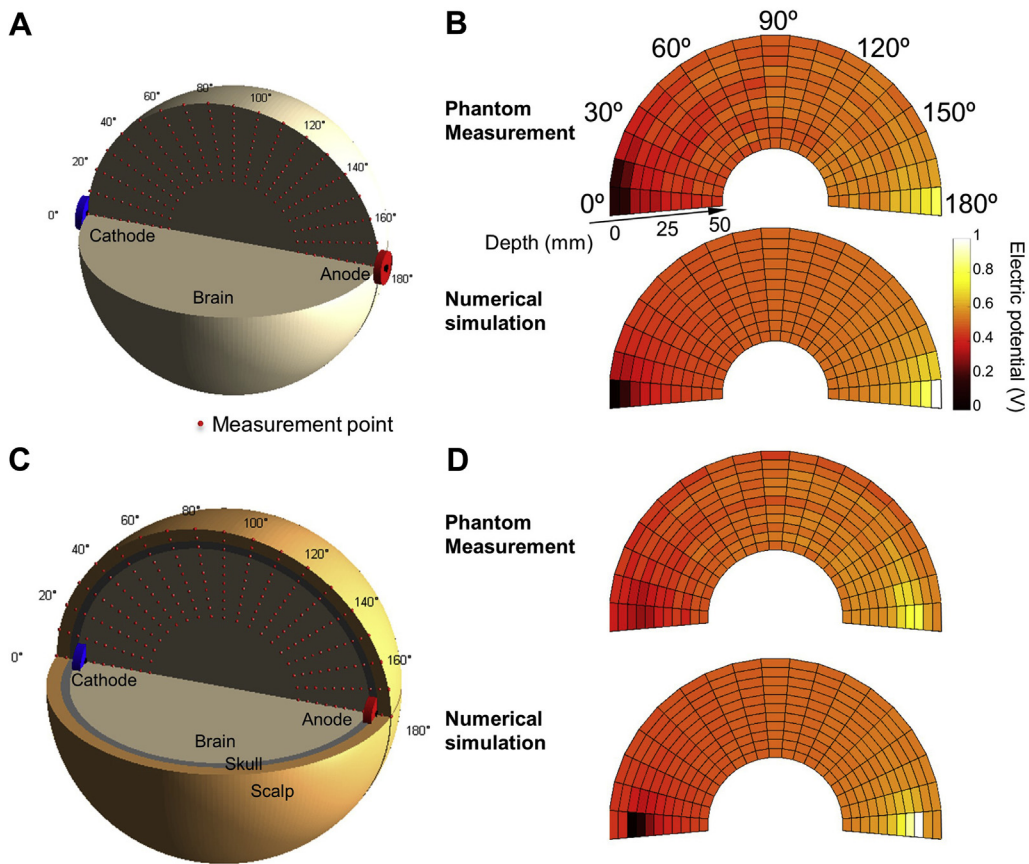


Figure 5. (A) Measurement points (red dots) for the one-layered spherical head model; (B) Color density map showing the comparison between the empirical and computed potentials in the one-layered spherical head model; (C) Measurement points (red dots) for the three-layered spherical head model, and (D) Color density map describing the comparison between measured and computed potentials in the three-layered spherical head model. (For interpretation of the references to color in this figure legend, the reader is referred to the web version of this article.)

Results

Spherical phantom heads

In this section, the validation study was conducted for one-/three-layered spherical phantom heads; thus, the electric potentials computed were compared to those measured empirically at various points on/inside the head. Figure 5 shows the comparison between the experimental and theoretical electric potential distributions—i.e., a direct comparison between empirical measurements with phantom heads and computational solutions of the Laplace boundary value problem described in Equations (1–4). Electric potentials were measured at 209 points per phantom, which can be expressed in spherical coordinates as: $\{(\rho, \theta, \phi) | \rho = 28.3, 33.3, 38.3, \dots, 78.3 \text{ mm}, \theta = 0^\circ, \phi = 0^\circ, 10^\circ, 20^\circ, 30^\circ, \dots, 180^\circ\}$ in the one-layered phantom head, and $\{(\rho, \theta, \phi) | \rho = 40, 45, 50, \dots, 90 \text{ mm}, \theta = 0^\circ, \phi = 0^\circ, 10^\circ, 20^\circ, 30^\circ, \dots, 180^\circ\}$ in the three-layered head. Because we used a ring type electrode, we were able to measure the electric potential at the center of the electrode ($\phi = 0^\circ$ and 180°). All measurement points are illustrated in detail in Fig. 5. One can see in Fig. 5 that the computational electric potential distributions were quite consistent with those measured empirically. The maximum differences in the potential distributions were approximately 0.17 V (one-layered) and 0.33 V (three-layered); the average relative differences between the measured and computed potentials were approximately 5.41% (one-layered) and 4.96% (three-layered). The relative difference was defined as $(|\text{Measured Potential} - \text{Computed Potential}| / |\text{Measured Potential}|) \times 100$. Electric potentials changed rapidly around the

electrodes and changed slowly at points distant from them. At the deeper measurement points, the electric potentials were more stable, as shown in Fig. 5. Overall, the electric potentials were quite homogenous, presumably because of the simple geometry of the spherical phantom heads. Further, with the exception of the areas around the electrodes, the discrepancies between the one- and three-layered spherical head models were not significant. From this observation, we concluded that the influence of the skull and scalp layers may be quite small in SuCS because of the very low conductivity of the skull relative to the brain (brain/skull = 17.8/1). Fully detailed comparative results are presented in Supplementary Figs. S2 and S3.

In particular, we investigated the variation in the angles between the anode and cathode in the one-layered spherical phantom. Figure 6 shows the comparison between the experimental and computational results at an electrode angle of 29.3°. For the other two electrode angles (43.9° and 58.5°), comparative results are illustrated in Supplementary Figs. S4 and S5. We observed that the potential difference was relatively high around the electrodes, while there was no remarkable distinction associated with the angle of the electrodes. Overall, the average relative differences (5.18% (29.3°), 5.21% (43.9°), 5.41% (58.5°)) were comparable, even though they increased slightly as the angle increased.

MRI-based phantom head

In this section, we used the three-layered realistic phantom head based on human MRI data to validate the computational

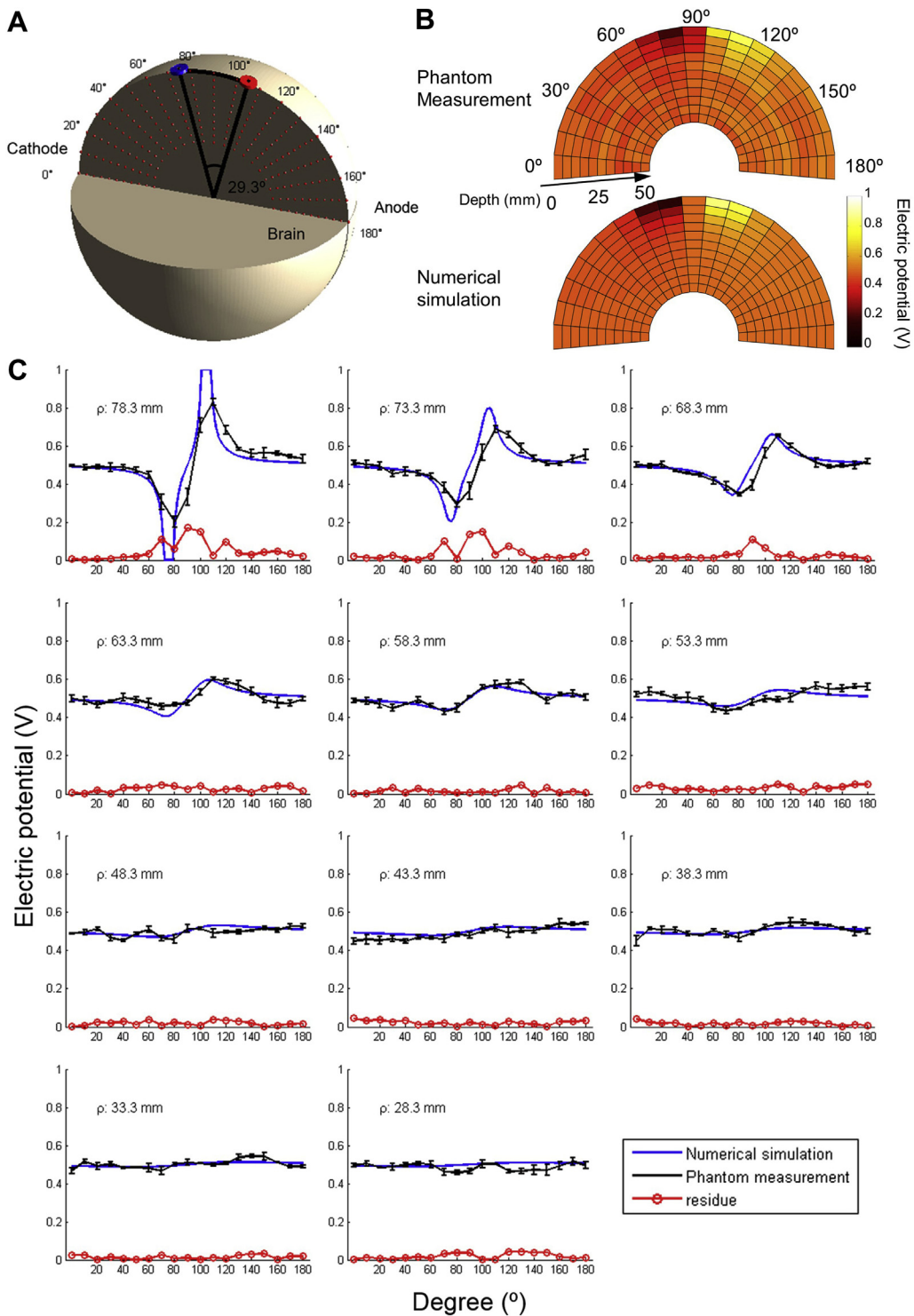


Figure 6. (A) Measurement point (red dots) for the one-layered spherical head model (arc length:40 mm, central angle:29.3°); (B) Color density map showing the comparison between the empirical and computed potentials, and (C) overall comparison between the numerical simulation and experimental results for the one-layered spherical head model. The bars represent SDs. (For interpretation of the references to color in this figure legend, the reader is referred to the web version of this article.)

electric potential distribution. Similar to the work on the spherical phantom heads, a total of 165 measurement points were taken from the scalp surface (depth of 0 mm) to the deep subcortical area (depth of 70 mm) in the mid-coronal plane of the head, as shown in Fig. 7A. For the 165 points, a comparison of the computational and empirically measured electric potential distributions is illustrated in Fig. 7B. Similar to the spherical phantom heads, the

measured and computed potential distributions behaved quite consistently; however, their discrepancy was relatively high around the electrodes. By comparison with the potential distribution in the spherical phantom heads, the electric potentials varied more across the measurement points; this may be due to the greater complexity of the MRI-based phantom head. The maximum discrepancy was 0.37 V, which occurred near the electrodes, as shown in Fig. 7B.

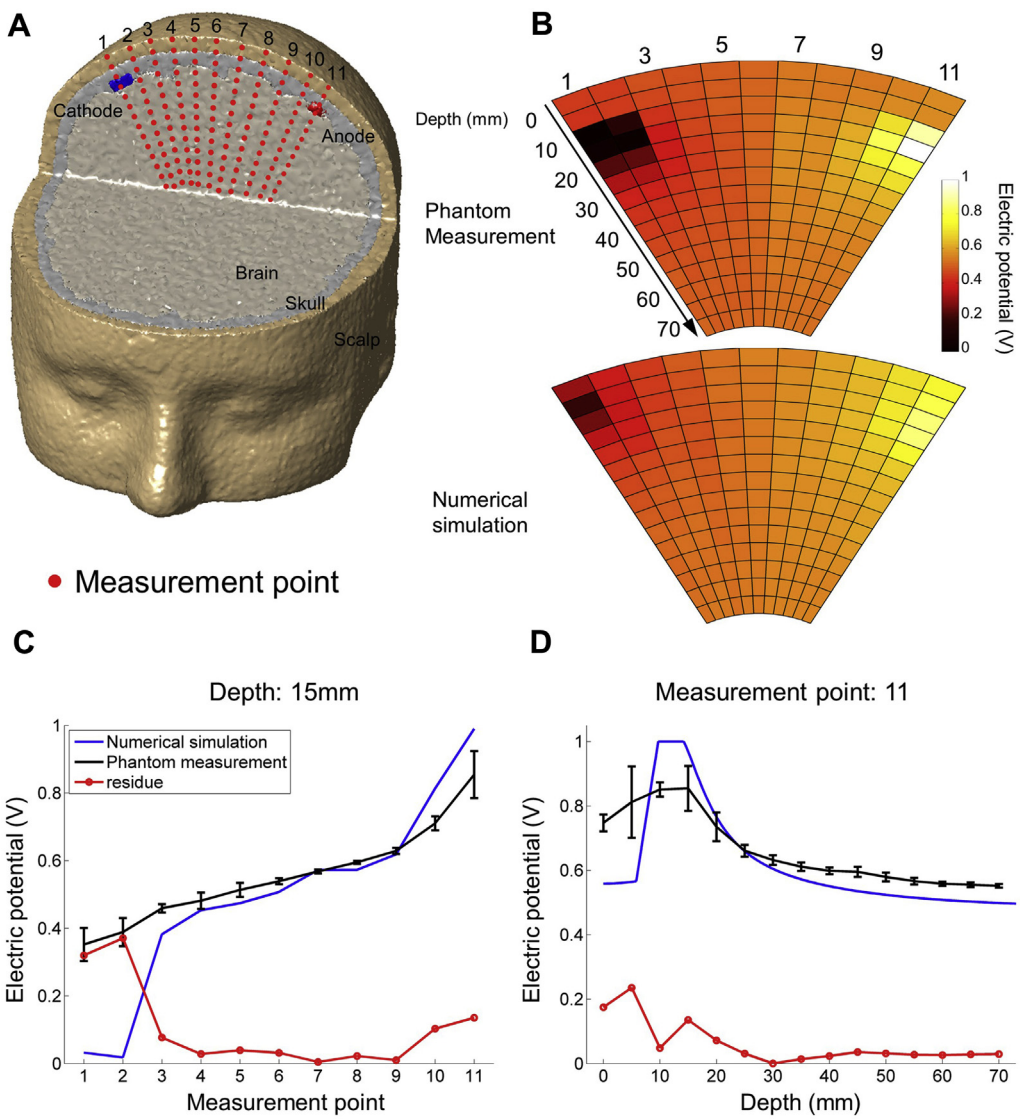


Figure 7. (A) Description of the three-layered MRI-based head model and 165 measurement points; (B) Color density map comparing 165 measured and computational electric potentials; (C) Measured and computed potentials at a depth of 10 mm, and their residues, and (D) Measured and computed potentials along the line (measurement point 11) passing the anode electrode (from surface to depth of 70 mm), and their residues. (For interpretation of the references to color in this figure legend, the reader is referred to the web version of this article.)

Taking into account the potential behavior along the arc line at a depth of 15 mm (close to the electrodes), the potential differences (residues) were considerably higher around the cathode than around the anode, as shown in Fig. 7C. Further, for various depth changes (at measurement point 11) the potential differences were high around the superficial area, including the electrode, while the potential differences became negligibly small in the subcortical area. Further, a potential peak occurred at a depth of 15 mm for both the measured and computed potentials, as shown in Fig. 7D. The average relative difference was approximately 10.3%; detailed results of the comparisons are shown in Supplementary Fig. S6.

An electric field were approximated based on 165 points of electric potential in the MRI-based phantom head and compared with those from the computational model, as shown in Fig. 8. We note that, due to insufficient measurement points, the current direction was estimated roughly, and the length of the arrow represents its magnitude. Similar to the potential distributions, electric field differences (mismatch of arrows) were quite high around the electrodes and decreased farther away. Around the boundaries of

the measurement region, differences were relatively higher because of the problem of a small sample of data points. However, the overall behavior between measured and computed electric field was quite similar and correlated reasonably well. The average difference in the current flow angles was 28.2°.

Discussion

Studies of phantom heads for validation purposes

In recent years, as high-performance computing techniques have allowed rapid increases in computational power and scalability, computational approaches have begun to provide new perspectives in a number of fields. In particular, computational studies of EBS are quite promising and advantageous, in that they are far more cost-effective and risk-free by comparison to human or animal studies. Further, even though there are several critical factors to be determined in order to achieve optimal EBS treatment, human case studies are too few and limited to address these factors

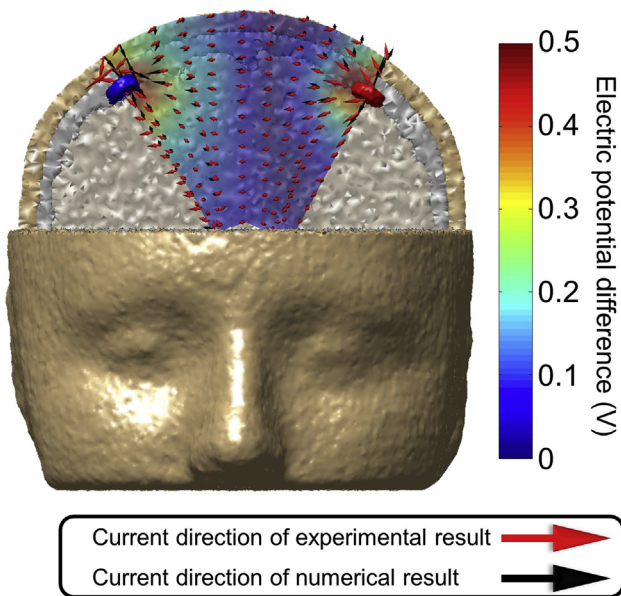


Figure 8. Comparison between experimental and computational results in the three-layered MRI-based head model. Arrows indicate the magnitude (log scale) and direction of the electric field (red: experimental results, black: computational results). The absolute difference in electric potentials between the results is illustrated in the background as a color density map. (For interpretation of the references to color in this figure legend, the reader is referred to the web version of this article.)

in a reasonable manner. Fortunately, computational studies may overcome such inherent obstacles, and at a lower cost. However, one problem presented by computational studies is that they require reasonable validation. In general, validation studies are employed to ensure that empirical and computational (expected) data behave consistently and vary within an acceptably small range. For such purposes, phantom studies are a common practice in medicine when human/animal studies cost too much or may not be applicable. Following such reasoning, we investigated three phantom heads (two spherical and an MRI-based phantom) in this work.

For each phantom head, a corresponding computational head model was generated to reduce as much as possible the discrepancy between the real phantom and the computational model. In this work, we achieved average relative differences (electric potentials) of about 5.4% and 10.3% for the three-layered spherical models and the MRI-based head model, respectively, which has been deemed to be quite a reasonable validation. Even the MRI-based head model showed only a slightly higher relative difference to those found in existing validation studies (tDCS phantom study [38]: 6% for just four measurement points, Pyrex phantom [39]: 5%). Thus, this technique may be quite promising, in that electric potentials were measured and compared at 209 or 165 points located both inside the head and on the head surface. In our early study [40] (reported at the conference), we observed that MRI-based phantom heads yielded quite good agreement with computational results at 39 shallow points (up to a depth of 20 mm corresponding to scalp, skull and cortical areas). To achieve better confidence in the results, it should have conducted with repeated measurement. However, in this study, substantially intensive and extensive validation was performed with a far larger number of measurement points (165) that considered the subcortical area (up to a depth of 70 mm). Moreover, two spherical phantoms resembling the human head structure were also tested extensively. Thus, to the best of our knowledge, this work may be the first extensive validation study of invasive subdural/epidural cortical stimulation.

Comparison of spherical and MRI-based head models

The comparison between the one- and three-layered spherical head models was interesting. With the two spherical head models, we could investigate how one-layered (brain layer only) and three-layered (brain, skull, and scalp layers) spherical models differ in terms of potential distributions induced by SuCS. Notably, we found that the differences between them were quite small, except for areas near the electrodes; SuCS may inherently stimulate the cortical area directly; thus, it is expected that the effect of current flowing out of the skull will be quite minimal. In this respect, from observations of only the one-layered spherical phantom head (brain layer only), we may infer the electric potential behavior in the three-layered spherical phantom. This is quite interesting, in that the one-layered spherical phantom can be manufactured much more easily. Thus, various SuCS electrode configurations in the one-layered (brain) spherical model may be tested at a modest cost because of the ease of implantation of the electrodes. Thereafter, the three-layered model may be inferred simply from the one-layered model; various electrode configurations for such one-layered cases are presented in the results and supplement sections.

The difference in the two three-layered head models (spherical and MRI-based computational model) is the degree to which they are able to represent the effects of the extent of cortical folding. By comparing these two models, we were able to investigate to what degree cortical folding influences electric potential distributions. In Fig. 9A and B, we observed that the potential difference at some distance from the electrodes and the difference in the electric fields near the electrodes may be the result of cortical folding; thus, the effects of cortical folding seem to be non-negligible. A notable potential difference in the deep subcortical area beneath the anodal electrode was likely captured by the tests of the MRI-based phantom, while a sharp difference in the electric fields near electrodes was not clearly captured; this was shown in Fig. 9C and D; this means that MRI-based phantom may capture partially cortical folding effect.

Assessment of averaged conductivity effect

In computational studies of EBS, it is common practice to introduce averaged conductivity in each layer. However, in reality, conductivities in the head or brain vary over the whole head, depending on neuron type, life or death of a neuron, and even stimulation frequency; thus it is difficult, if not impossible, to estimate various conductivity distributions within the head accurately. For this reason, we may raise an interesting question—is it acceptable in computational studies to assign averaged homogeneous conductivity values rather than true inhomogeneous conductivity distributions? For this purpose, the electric potential/electric field behavior of several averaged conductivity ratios (brain:skull:scalp) in the computational, MRI-based head model was investigated and compared with the electric potential data measured empirically in the MRI-based phantom head. Our phantom head was manufactured to have almost homogenous conductivity values for each layer. However, in reality, it may have an inhomogeneous conductivity distribution to some extent due to limitations in manufacturing skills. Thus, our phantom may be considered an inhomogenous model and used to assess the averaged conductivity effect. Because of their simplicity, the averaged conductivity ratios introduced in the MRI-based head model were considered as a baseline (a reference ratio was set as brain:skull:scalp = 17.8:1:39.2 in this study). Then, the conductivity of one layer (brain, skull, or scalp) was allowed to vary, while the other two layers remains fixed. Figure 10 shows electric potential and electric field behaviors for various conductivity ratios at

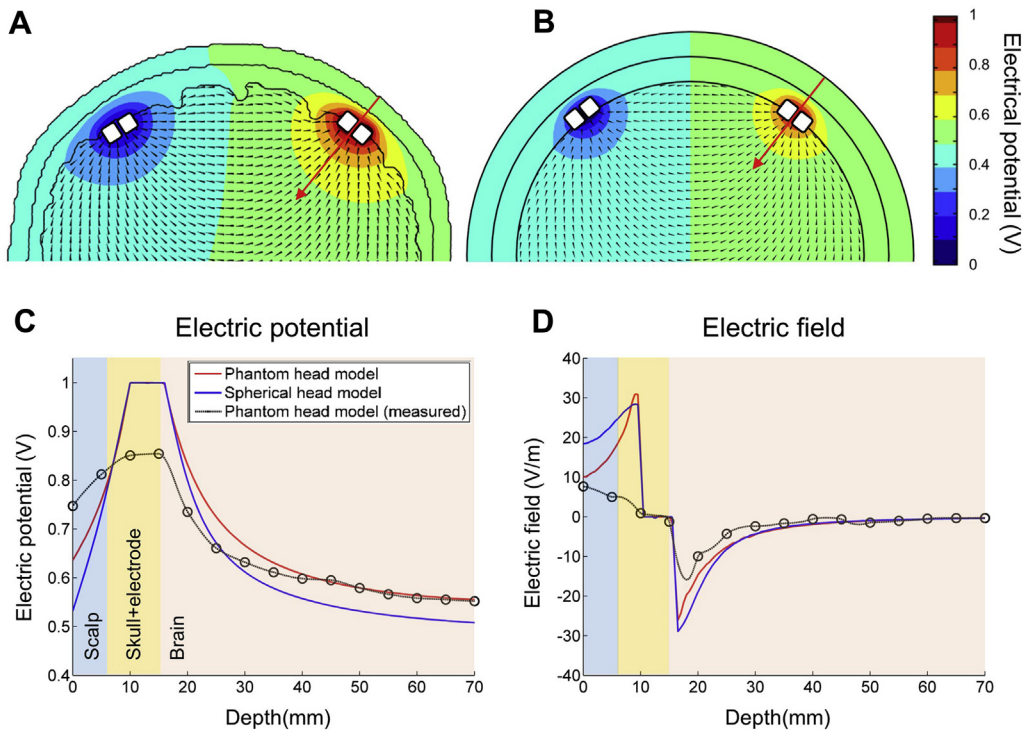


Figure 9. Comparison of electric potential and electric field between two computational models (MRI-based and three-layered spherical models) under the same electrode configuration. This difference represents cortical folding effect. (A) Electric potential distribution and electric field of computational MRI-based head model, (B) spherical head model, (C) and empirical MRI-based phantom head. Electric potential and electric field behaviors over varying depth right beneath anodal electrode (D).

varying depths immediately beneath the anodal electrode (corresponding to measurement 11 in Fig. 9A). We found that, for the case of fixed scalp and skull conductivity ratios, two extreme ratios (brain:skull:scalp = 1:1:39.2 or 5:1:39.2) relative to our MRI-based phantom (brain:skull:scalp = 17.8:1:39.2) yielded notable differences in potential and electric fields. These potential differences were considerably higher in the subcortical brain (farther from the electrode) than were those between the measured and computed potentials. Further, most computational models yielded comparable sharp electric field (EF) changes around the electrode. However, the EFs derived from the empirical data exhibited behavior that had a strong, positive correlation with the computed EF, while they showed relatively small change near the electrode. In the case of fixed brain and scalp conductivity ratios, one extreme ratio (brain:skull:scalp = 17.8:10:39.2) yielded clear differences in potentials and electric fields.

From these results, we observed that potentials measured in the MRI-based phantom head were correlated highly with the computational potentials. Computational data tell us that averaged variations in conductivity may yield some degree of variation in potentials and electric fields, while only extreme cases will yield notable differences. However, differences between the MRI-based phantom and its corresponding computational model were, overall, larger than were the differences induced by variations in conductivity, except for potential differences in a few extreme cases. In conclusion, we suggest that averaged conductivities may play a role in determining typical behavior potentials or electric fields; however, it is likely that the effect of variations in conductivity is small relative to that of probable measurement errors. Simple estimations or the use of averaged conductivity values would have some mild effect on stimulation; thus, use of averaged conductivity values (conventional conductivity values) in computational studies may be acceptable when trying to avoid unreasonably extreme cases.

Causes of differences between phantom and computational results

Empirical measures from our three phantom studies were compared with their corresponding computational models. All electric potentials (measured and computed) showed good agreement (average relative difference: approximately 5.4% for three-layered spherical phantoms, and 10.3% for MRI-based phantom). In proximity to the stimulation electrodes, we observed overall relatively higher differences. We believe that three possible factors may cause such differences. First, unavoidably small displacements of measurement points could make a difference. For the MRI-based phantom head, 11 measurement points were selected on the scalp layer. For each scalp point, an additional 14 measurement points were selected manually along the line from the point of the scalp toward the subcortical region. Because it is inevitable that there will be measurement errors in these lines, as well as in the positioning of the measurement points, these factors may yield a larger displacement discrepancy between the computational and experimental models for deeper measurement points. This unavoidable error in the displacement of measurement points may have a greater influence in the MRI-based phantom study. Due to the inherent complexity of its geometry, electric potential distributions were less trivial and more difficult to measure in the MRI-based phantom study than in the spherical phantom head studies; thus, this may account in part for the asymmetry in Fig. 7C. According to the literature [29,38,39], electric potentials measured on phantoms are not terribly accurate because of poor spatial placement of the measuring sensor (probe). Thus, to reduce the displacement error in measurement points, we recommend the use of a coordinate-based measuring machine or a guided computed-tomography (CT) image of the phantom with a sensor attachment [41].

Second, we observed that solidification of the Agar/NaCl mixture left a film of water on the surface of each phantom compartment

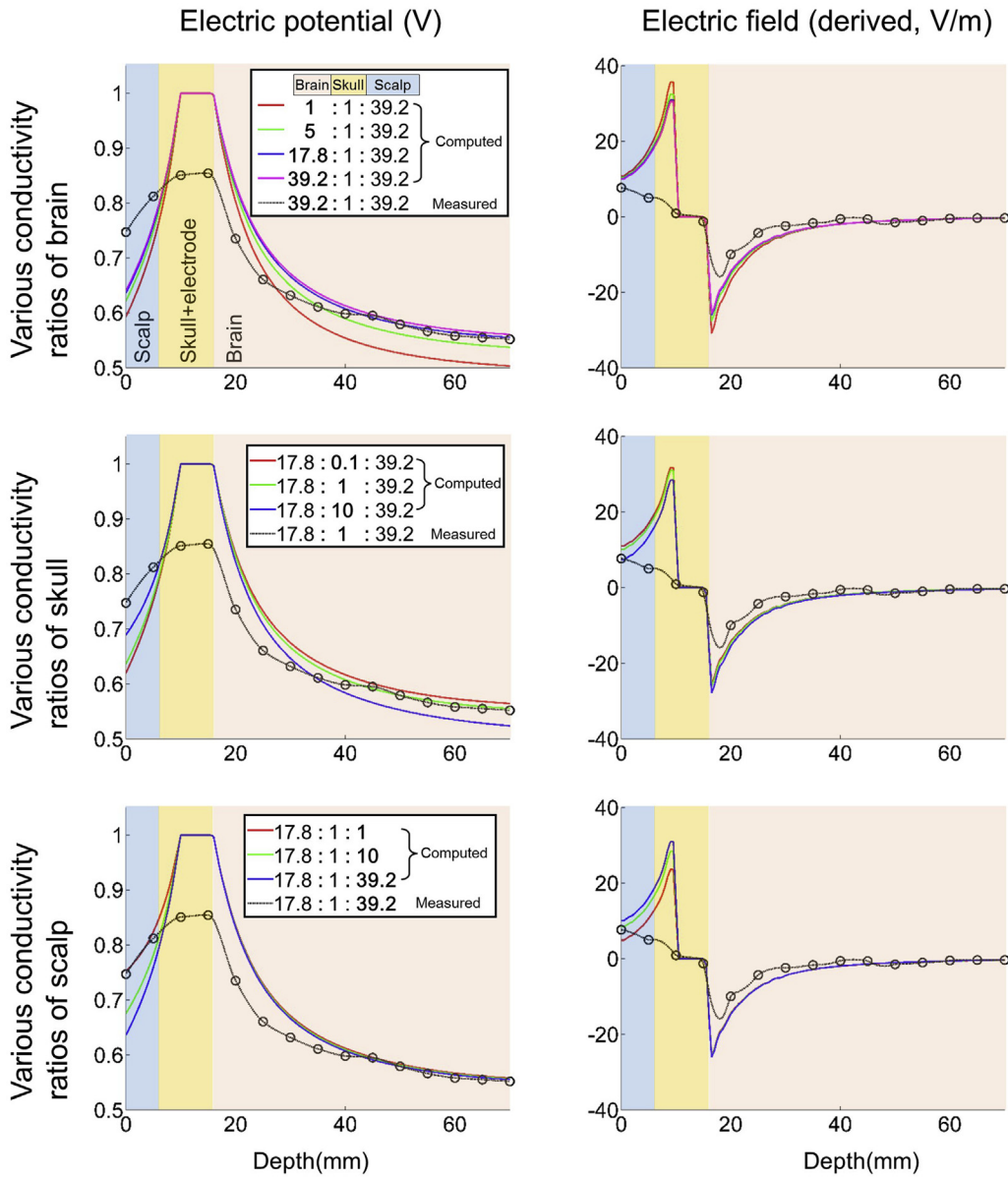


Figure 10. Comparison of electric potential and electric field with respect to various brain:skull:scalp conductivity ratios. In each row, one conductivity ratio was varied, otherwise the other two conductivity ratios were fixed (base conductivity ratio of brain:skull:scalp = 17.8:1:39.2).

(scalp, skull, and brain layers). This may change the material properties of the phantom slightly, thereby causing errors in the potential differences. To avoid this, we dried all surfaces thoroughly during assembly of each phantom. However, we still observed that the film of water continued to form over time, and its complete removal was nearly impossible.

Third, the discrepancy in the positioning of the electrodes between the phantom and computational models is minor, but it may be a possible factor in the potential differences. We injected current into the brain through electrodes; thus, the magnitude of electric potentials around the electrodes was significantly higher than that in other regions, which indicates that even minor discrepancies in positioning may yield significant differences in potentials. In this work, after manufacturing the phantom heads, we generated computational models to reduce mismatch as much as possible between the phantom and computational models. However, minute mismatches were unavoidable.

Lastly, in the computational study, we assumed that the electrode-tissue interface is generally modeled in complete contact. However, in a practical environment, the electrode-tissue interface may be not be in good contact due to curvature of the gyri, the flexibility of the stimulation electrodes, or hair in the tDCS. Even in our study, these possible factors may be reflected significantly, thereby causing notable discrepancies around the electrodes and asymmetric behavior in the MRI-based phantom model. For a complete understanding of these factors, including the effect of incomplete contact, our group is pursuing further studies of these issues.

The implications of phantom validation studies

For the purposes of validation, we constructed phantom heads in this work. These phantoms may have great potential in validating other neuromodulation techniques as well. Most

neuromodulation techniques are based on electrical stimulation, with or without electrodes, and thus our phantom manufacturing approaches, in which we used Agar/NaCl mixtures to control the electric conductivity values, may be applied easily to other EBSs. In addition, it may be possible to validate the thermal effects generated commonly during EBS by adjusting the aluminum powder/NaCl mixtures to control thermal conductivity [42]. Finally, it has been suggested that the validation of computational studies for optical stimulation or optogenetics may be achieved with phantom materials with similar light-scattering properties in the brain tissue.

Remained issues and future direction

The goal of this work was to validate the feasibility of computational models for EBS, in particular, SuCS. Even though we used phantoms in this work for extensive validation of invasive cortical stimulation, the following limitations must be addressed. Some of the issues have been discussed in detail above. In addition to those, however, our MRI-based phantom head was generated with three layers that represented the scalp, skull, and brain due to the complicated procedure of phantom assembly. Recent computational studies on EBS have introduced MRI-based human models consisting of more than five layers (scalp, skull, gray matter, white matter, and cerebrospinal fluid components). In particular, the thicknesses of cerebrospinal fluid and gray matter are considered to measure approximately 1.0 mm and 2.5 mm, respectively. We found that these are too thin to generate in our MRI-based phantom head model. Thus, in our phantom, we could not measure the practical shunting and interface effects in the CSF layer, as well as at the CSF-GM boundary, even though these effects may be considered in computational studies.

In one phantom study [30], five layers were considered, but unrealistic smooth shapes were introduced in the gray and white matter layers. Thus, it is a challenge to manufacture a more detailed phantom head. Further, most computational studies of EBS commonly investigate the distribution of current density or electric fields in the brain, because the excitability of neurons is linearly proportional to the magnitude of the current density or electric field [43,44]. In this work, the electric field was estimated roughly from fewer measurement points. Accurate estimation of electric field/current density at proper spatial resolution was not possible in this study, as errors in the measurement of potentials are unavoidable and influence the estimation procedure greatly. Moreover, discrepancies in the electrode-tissue interface in phantom and computational studies constitute another hurdle. In computational modeling, it is assumed that the electrode-tissue interface is in complete contact. However, in reality, this may not be the case. In SuCS, the curvature of the gyri results in less complete contact. These discrepancies are unavoidable and their effects should be investigated thoroughly. Lastly, our validation study was limited to phantoms; even the realistic MRI-based phantom was constructed, and thus, we cannot guarantee that it is directly applicable to a human. However, this work does tell us that computational studies that employ more detailed head modeling are more likely to resolve the questions pertaining to EBS that remain to be answered. For example, what degree of head model mismatch (including compartments, conductivity values, segmentation precision, and so on) is acceptable in computational studies that attempt to assess the effects of EBS? We hope that this work contributes to the resolution of such questions; thus it is eventually beneficial in finding the optimal EBS procedure for clinical purpose.

Conclusions

In this work, we manufactured one/three-layered spherical phantom heads and a three-layered MRI-based phantom, and compared their computational and empirical electric potentials. We found that computed and measured electric potentials behaved consistently, with relative differences of approximately 5% (spherical models) and 10% (MRI-based model), respectively. From this investigation, we suggest that computational studies may be validated reasonably with various phantom models. Moreover, our MRI-based phantom manufacturing approaches may have the potential to validate computational studies of other types of EBS techniques.

Appendix. Supplementary data

Supplementary data related to this article can be found online at <http://dx.doi.org/10.1016/j.brs.2015.06.009>

References

- [1] Moro E, Schwall JM, Piboolnurak P, et al. Unilateral subdural motor cortex stimulation improves essential tremor but not Parkinson's disease. *Brain* 2011;134:2096–105. <http://dx.doi.org/10.1093/brain/awr072>.
- [2] Kim H-I, Shin Y-I, Moon S-K, Chung G-H, Lee M-C, Kim H-G. Unipolar and continuous cortical stimulation to enhance motor and language deficit in patients with chronic stroke: report of 2 cases. *Surg Neurol* 2008;69:77–80. <http://dx.doi.org/10.1016/j.surneu.2006.12.055>. discussion 80.
- [3] Garcia-Larrea L, Peyron R, Mertens P, et al. Electrical stimulation of motor cortex for pain control: a combined PET-scan and electrophysiological study. *Pain* 1999;83:259–73.
- [4] Benabid AL, Pollak P, Gao D, et al. Chronic electrical stimulation of the ventralis intermedius nucleus of the thalamus as a treatment of movement disorders. *J Neurosurg* 1996;84:203–14. <http://dx.doi.org/10.3171/jns.1996.84.2.0203>.
- [5] Canavero S, Paolotti R, Bonicalzi V, et al. Extradural motor cortex stimulation for advanced Parkinson disease. Report of two cases. *J Neurosurg* 2002;97:1208–11. <http://dx.doi.org/10.3171/jns.2002.97.5.1208>.
- [6] Katayama Y, Fukaya C, Yamamoto T. Control of poststroke involuntary and voluntary movement disorders with deep brain or epidural cortical stimulation. *Stereotact Funct Neurosurg* 1997;69:73–9. <http://dx.doi.org/10.1159/000099855>.
- [7] Morrell MJ. Responsive cortical stimulation for the treatment of medically intractable partial epilepsy. *Neurology* 2011;77:1295–304. <http://dx.doi.org/10.1212/WNL.0b013e3182302056>.
- [8] Nahas Z, Anderson BS, Borckardt J, et al. Bilateral epidural prefrontal cortical stimulation for treatment-resistant depression. *Biol Psychiatry* 2010;67:101–9. <http://dx.doi.org/10.1016/j.biopsych.2009.08.021>.
- [9] Cherney LR, Harvey RL, Babbitt EM, et al. Epidural cortical stimulation and aphasia therapy. *Aphasiology* 2012;26:1192–217. <http://dx.doi.org/10.1080/02687038.2011.603719>.
- [10] Franzini A, Ferroli P, Servello D, Broggi G. Reversal of thalamic hand syndrome by long-term motor cortex stimulation. *J Neurosurg* 2000;93:873–5.
- [11] Gao F, Wang S, Guo Y, et al. Protective effects of repetitive transcranial magnetic stimulation in a rat model of transient cerebral ischaemia: a microPET study. *Eur J Nucl Med Mol Imaging* 2010;37:954–61. <http://dx.doi.org/10.1007/s00259-009-1342-3>.
- [12] Aydin-Abidin S, Trippel J, Funke K, Eysel UT, Benali A. High- and low-frequency repetitive transcranial magnetic stimulation differentially activates c-Fos and zif268 protein expression in the rat brain. *Exp Brain Res* 2008;188:249–61. <http://dx.doi.org/10.1007/s00221-008-1356-2>.
- [13] Florio T, Scarnati E, Confalone G, et al. High-frequency stimulation of the subthalamic nucleus modulates the activity of pedunculopontine neurons through direct activation of excitatory fibres as well as through indirect activation of inhibitory pallidal fibres in the rat. *Eur J Neurosci* 2007;25:1174–86. <http://dx.doi.org/10.1111/j.1460-9568.2007.05360.x>.
- [14] Garcia-Larrea L, Peyron R. Motor cortex stimulation for neuropathic pain: from phenomenology to mechanisms. *Neuroimage* 2007;37(Suppl.1):S71–9. <http://dx.doi.org/10.1016/j.neuroimage.2007.05.062>.
- [15] Levy R, Ruland M, Weinand M, Lowry D, Dafer R, Bakay R. Cortical stimulation for the rehabilitation of patients with hemiparetic stroke: a multicenter feasibility study of safety and efficacy. *J Neurosurg* 2008;108:707–14. <http://dx.doi.org/10.3171/JNS/2008/108/4/0707>.
- [16] Deng Z-D, Lisanby SH, Peterchev AV. Electric field strength and focality in electroconvulsive therapy and magnetic seizure therapy: a finite element simulation study. *J Neural Eng* 2011;8:016007. <http://dx.doi.org/10.1088/1741-2560/8/1/016007>.

- [17] Datta A, Elwassif M, Battaglia F, Bikson M. Transcranial current stimulation focality using disc and ring electrode configurations: FEM analysis. *J Neural Eng* 2008;5:163–74. <http://dx.doi.org/10.1088/1741-2560/5/2/007>.
- [18] Wongsarnpigoon A, Grill WM. Computational modeling of epidural cortical stimulation. *J Neural Eng* 2008;5:443–54. <http://dx.doi.org/10.1088/1741-2560/5/4/009>.
- [19] Wongsarnpigoon A, Grill WM. Computer-based model of epidural motor cortex stimulation: effects of electrode position and geometry on activation of cortical neurons. *Clin Neurophysiol* 2012;123:160–72. <http://dx.doi.org/10.1016/j.clinph.2011.06.005>.
- [20] Zwartjes DG, Heida T, Feirabend HK, et al. Motor cortex stimulation for Parkinson's disease: a modelling study. *J Neural Eng* 2012;9:056005. <http://dx.doi.org/10.1088/1741-2560/9/5/056005>.
- [21] Datta A, Baker JM, Bikson M, Fridriksson J. Individualized model predicts brain current flow during transcranial direct-current stimulation treatment in responsive stroke patient. *Brain Stimul* 2011;4:169–74. <http://dx.doi.org/10.1016/j.brs.2010.11.001>.
- [22] Opitz A, Windhoff M, Heidemann RM, Turner R, Thielscher A. How the brain tissue shapes the electric field induced by transcranial magnetic stimulation. *Neuroimage* 2011;58:849–59. <http://dx.doi.org/10.1016/j.neuroimage.2011.06.069>.
- [23] Thielscher A, Opitz A, Windhoff M. Impact of the gyral geometry on the electric field induced by transcranial magnetic stimulation. *Neuroimage* 2011;54:234–43. <http://dx.doi.org/10.1016/j.neuroimage.2010.07.061>.
- [24] Kim D, Seo H, Kim H, Jun S. Computational study on subdural cortical stimulation—the influence of the head geometry, anisotropic conductivity, and electrode configuration. *PLoS One* 2014;9. <http://dx.doi.org/10.1371/journal.pone.0108028>.
- [25] Wagner T, Fregni F, Eden U, et al. Transcranial magnetic stimulation and stroke: a computer-based human model study. *Neuroimage* 2006;30:857–70. <http://dx.doi.org/10.1016/j.neuroimage.2005.04.046>.
- [26] Rattay F. The basic mechanism for the electrical stimulation of the nervous system. *Neuroscience* 1999;89:335–46.
- [27] Rattay F. Analysis of models for external stimulation of axons. *IEEE Trans Biomed Eng* 1986;33:974–7.
- [28] Seo H, Kim D, Jun SC. Comparison of neuronal excitation between extruded slab partial head model and full head model in subdural cortical stimulation. *Conf Proc IEEE Eng Med Biol Soc* 2013;241–4.
- [29] Wei XF, Grill WM. Current density distributions, field distributions and impedance analysis of segmented deep brain stimulation electrodes. *J Neural Eng* 2005;2:139–47. <http://dx.doi.org/10.1088/1741-2560/2/4/010>.
- [30] Kim D-H, Choi N-S, Won C, Georgiou GE. Distortion of the electric field distribution induced in the brain during transcranial magnetic stimulation. *IET Sci Meas Technol* 2010;4:12. <http://dx.doi.org/10.1049/iet-smt.2008.0159>.
- [31] Song W, Truong DQ, Bikson M, Martin JH. Trans-spinal direct current stimulation immediately modifies motor cortex sensorimotor maps. *J Neurophysiol* 2015;113:2801–11. <http://dx.doi.org/10.1152/jn.00784.2014>.
- [32] Datta A, Zhou X, Su Y, Parra LC, Bikson M. Validation of finite element model of transcranial electrical stimulation using scalp potentials: implications for clinical dose. *J Neural Eng* 2013;10:036018. <http://dx.doi.org/10.1088/1741-2560/10/3/036018>.
- [33] Han X, Fischl B. Atlas renormalization for improved brain MR image segmentation across scanner platforms. *IEEE Trans Med Imaging* 2007;26:479–86. <http://dx.doi.org/10.1109/TMI.2007.893282>.
- [34] Smith SM. Fast robust automated brain extraction. *Hum Brain Mapp* 2002;17:143–55. <http://dx.doi.org/10.1002/hbm.10062>.
- [35] Bennett D. NaCl doping and the conductivity of agar phantoms. *Mater Sci Eng C* 2011;31:494–8. <http://dx.doi.org/10.1016/j.msec.2010.08.018>.
- [36] Datta A, Bansal V, Diaz J, Patel J, Reato D, Bikson M. Gyri-precise head model of transcranial DC stimulation: Improved spatial focality using a ring electrode versus conventional rectangular pad. *Brain Stimul* 2009;2:201–7. <http://dx.doi.org/10.1016/j.brs.2009.03.005>.
- [37] Zhang Z. A fast method to compute surface potentials generated by dipoles within multilayer anisotropic spheres. *Phys Med Biol* 1995;40:335–49. <http://dx.doi.org/10.1088/0031-9155/40/3/001>.
- [38] Jung Y-J, Kim J-H, Kim D, Im C-H. An image-guided transcranial direct current stimulation system: a pilot phantom study. *Physiol Meas* 2013;34:937–50. <http://dx.doi.org/10.1088/0967-3334/34/8/937>.
- [39] Suesserman MF, Spelman FA, Rubinstein JT. In vitro measurement and characterization of current density profiles produced by non-recessed, simple recessed, and radially varying recessed stimulating electrodes. *IEEE Trans Biomed Eng* 1991;38:401–8. <http://dx.doi.org/10.1109/10.81558>.
- [40] Jeong J, Kim D, Jeong S, et al. Validation of numerical simulation for subdural cortical stimulation: using spherical phantoms and anatomically realistic head phantom. *Bioinforma. 2014-5th Int. Conf. Bioinforma. Model. Methods Algorithms, Proceedings; Part 7th Int. Jt. Conf. Biomed. Eng. Syst. Technol. BIOSTEC 2014. SciTePress;* 2014. p. 136–41.
- [41] Leahy RM, Mosher JC, Spencer ME, Huang MX, Lewine JD. A study of dipole localization accuracy for MEG and EEG using a human skull phantom. *Electroencephalogr Clin Neurophysiol* 1998;107:159–73.
- [42] Leonard JB, Foster KR, Athey TW. Thermal properties of tissue equivalent phantom materials. *IEEE Trans Biomed Eng* 1984;31:533–6. <http://dx.doi.org/10.1109/TBME.1984.325296>.
- [43] Bikson M, Inoue M, Akiyama H, et al. Effects of uniform extracellular DC electric fields on excitability in rat hippocampal slices in vitro. *J Physiol* 2004;557:175–90. <http://dx.doi.org/10.1113/jphysiol.2003.055772>.
- [44] Radman T, Ramos RL, Brumberg JC, Bikson M. Role of cortical cell type and morphology in subthreshold and suprathreshold uniform electric field stimulation in vitro. *Brain Stimul* 2009;2:215–28. <http://dx.doi.org/10.1016/j.brs.2009.03.007>. 228.e1–3.